V International Conference on Particle-based Methods – Fundamentals and Applications
PARTICLES 2017
P. Wriggers, M. Bischoff, E. Oñate, D.R.J. Owen, & T. Zohdi (Eds)

ENHANCEMENT OF THE SPREADING PROCESS IN ADDITIVE MANUFACTURING THROUGH THE SPREADER OPTIMISATION.

S. Haeri[1]

[1] Department of Mechanical and Aerospace Engineering
75 Montrose St
University of Strathclyde
Glasgow
UK, G1 1XJ
E-mail: sina.haeri@strath.ac.uk

Key words: DEM, Powder Spreading, Additive Manufacturing, Particle Bed Fusion, Optimisation

Abstract. Powders used in Particle Bed Fusion (PBF) process are spread onto compact layers and then are sintered. This process is repeated layer by layer to form the final products. The author has recently characterised the process and it is found that spreading the particles with a counter-rotating roller produces a bed with higher qualities, i.e. lower void fractions and surface roughness [Powder Technology, 306 (2017) 45–54]. This is related to a particle dragging effect caused by the small contact area between powder grains and the blade. Therefore, here, it is postulated that changing the blade profile at the blade-bed contact point can significantly influence the contact dynamics and hence increase the blade's effectiveness as a spreading device for PBF. A set of computer simulations using Discrete Element Method (DEM) are performed at device scales to optimise the geometry of blade spreaders to yield the lowest void fraction and surface roughness. The blade profile is parametrised using a super-ellipse with three geometrical parameters. It is firstly demonstrated that geometric optimisation of a blade profile is an effective alternative to using more complex spreading devices. Secondly, for the proposed parametrisation, the optimum values are found using computer simulations which can generate very high quality powder beds with volume fractions close to the critical value.

1 INTRODUCTION

Powder Bed Fusion (PBS) is a promising Additive Manufacturing (AM) technology where polymeric or metallic particles, heated to just below their melting temperature are spread on a fabrication piston to form a thin powder bed (typically in the order of 0.1 mm) using a counter-rotating roller or a blade. Different technologies may then be used

to fuse the material powder. For example, in a Laser Sintering (LS) process, a laser beam is used to fuse the powder grains. After this stage, the fabrication piston lowers the part slightly and a new layer of powder is applied. The process is repeated until the product is fabricated [1].

Undoubtedly, the characteristics of individual particles have a significant effect on the success of PBF processes [2, 3, 4, 5]. In particular, Ziegelmeier [6] focused on understanding the bulk and flow behaviour of polymer powders in relation to the properties of produced parts in LS. They mainly concluded that the tensile strength and elongation at break are enhanced by increasing ϕ_s. Therefore, the discrete nature of particles cannot be ignored in any numerical technique used for design, prediction and understanding of PBF processes. The Discrete Element Method (DEM) is a particle based approach relying only on the first principles and is receiving significant attention recently for simulation of such systems. This is due to the capability of DEM to directly include the effects of grain characteristics such as material properties, size distribution and morphology. DEM was first proposed in late 1970s [7] and there is a large body of research on the method in geomechanics literature (see [8] for a modern introduction).

Application of DEM to PBF was pioneered by Zohdi [9, 10, 11] with regards to the development of laser heat sources and particle sintering models. Xiang et al. [12], simplified the process by considering an assembly of 4000 particles undergoing three processes in their DEM simulations: random packing, layering and compression. They showed that the solid volume fraction increases by increasing the layer thickness. Steuban et al. [13] also proposed a new framework for modelling the full process including a laser heat source and powder sintering. Lattice-Boltzmann models are also developed very recently to simulate the melting-solidification processes [14, 15]. However, they start from a random collection of spheres, rather that considering the full spreading process.

Haeri et al. [1] on the other hand provided DEM simulation of spreading process at *device scales* and used high ϕ_s and layer's surface roughness values as a measure of a successful powder spreading process (i.e. a high-quality bed). This is known to be directly correlated with the quality of final parts [6]. In their extensive parametric studies, Haeri et al. [1] investigated the effects of spreader type, its translational velocity, particle shape (and its distribution) and layer thickness on the bed quality. They parametrised elongated particles using their aspect ratios A_r and showed that the highest ϕ_s can be achieved at $\mathrm{A}_r = 1.5$. They also analysed the micro-structures of elongated particles to explain the relation between various process parameters and the bed quality. They investigated two different types of spreading devices: rollers and blades. The consensus in the community is that the rollers generally produce higher quality powder beds which was confirmed in this study. Haeri et al. [1] however, related this to a particle dragging phenomenon and a small contact area between a blade spreader and the bed.

In this paper, it is postulated that since a low-quality bed generated using a blade is essentially a result of its geometry – as was suggested in [1] – it can be rectified purely by geometric modification of the blade. Therefore, a new class of blades is proposed with

a modified head profile. The suggested profile is a supper-ellipse with three adjustable parameters. It is shown that simple geometrical modifications can significantly affect the bed quality and then using a series of computer simulations the best values for the these parameters are identified and reported.

2 Methodology

2.1 Discrete Element Method

The Large-scale atomic/molecular massively parallel simulator (LAMMPS) code [16] is used for all the DEM simulations. A linear Hookean spring-dashpot contact force model is applied to each pair of particles p and q whenever the two particles overlap, i.e. when $\delta_{pq} = R_p + R_q - r_{pq} > 0$, where $r_{pq} = \|\mathbf{r}_p - \mathbf{r}_q\|$, and $\|\cdot\|$ represents the Euclidean norm (magnitude) of any vector. In addition, R_k, $k \in \{p, q\}$, is the radius of the k^{th} spheroid and $\mathbf{r}_k$ is the position vector of its centre of mass (CoM). The normal and tangential components of spring-dashpot force are given by

$$\mathbf{F}^n = \kappa_n \delta_{pq} \mathbf{n}_{pq} - \gamma_n m^* \mathbf{v}^n_{pq} \tag{1}$$

$$\mathbf{F}^t = -\kappa_t \mathbf{u}^t_{pq} - \gamma_t m^* \mathbf{v}^t_{pq}, \tag{2}$$

where $\kappa_n, \gamma_n, \kappa_t$ and γ_t are spring elastic and damping constants in normal and tangential directions respectively. In addition, $\mathbf{v}^n_{pq}$ and $\mathbf{v}^t_{pq}$ are relative normal and tangential velocities. The effective mass is defined as $m^* = m_p m_q/(m_p + m_q)$ where m_k, $k \in \{p, q\}$, is the mass of k^{th} particle. The unit normal vector in the direction of the line connecting a pair of spheroid centres is presented by $\mathbf{n}_{pq}$ and elastic shear displacement by $\mathbf{u}^t_{pq}$. The tangential force is limited to $\|\mathbf{F}^t_{pq}\| \leq \mu_c \|\mathbf{F}^n_{pq}\|$ where μ_c is the Coulomb friction coefficient which is set to 0.5 in this study [1]. Similarly, a normal $\mathbf{F}^n_{pw}$ and a tangential force $\mathbf{F}^t_{pw}$ are defined between particle p and the bottom wall w.

Shape effects are considered in this paper and hence, a versatile multi-sphere technique is used [1]. In this paper, rod-shaped particles are considered which can be parametrised using an aspect ratio A_r. This is chosen since elongated particles with a similar aspect ratio distribution and round edges can be considered as approximations to a population of impact-milled PEEK particles [1]. In addition, rod-shaped particles with required aspect ratios of $\mathrm{A}_r = 1.5, 2.0, 2.5$ could be generated with 2, 3 and 4 spheroids, considerably reducing the costs of the computations. Therefore, these are used as approximations to the real particles for the optimisations stage where a large number of simulations are required.

The simulation set-up is depicted in Figure 1b. The bottom boundary is a rigid wall that exerts a normal and a tangential force on the particles (equivalent to assuming an infinity large sphere in Eqs. (1) and (2)). To prevent unbounded rotation of particles on the bottom wall, a rolling friction model is implemented [17, 18, 19]. The elastic spring constant κ_n, in Eq. (1) is set according to [20]. The coefficient of restitution is set to 0.5 and the values of Young's modulus, Poisson ratio and particle density are set to 3.7 GPa,

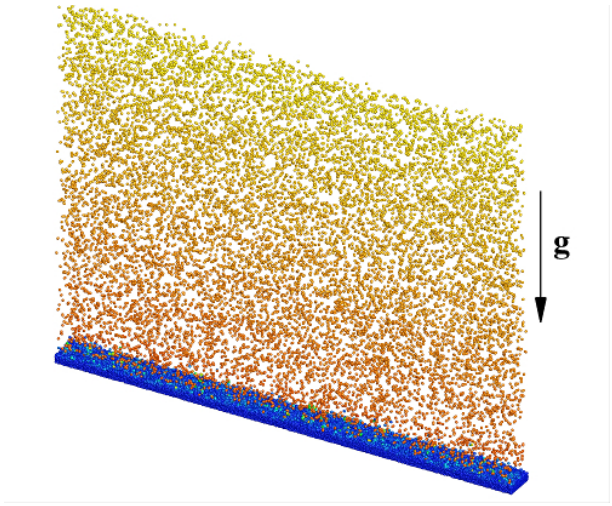

(a)

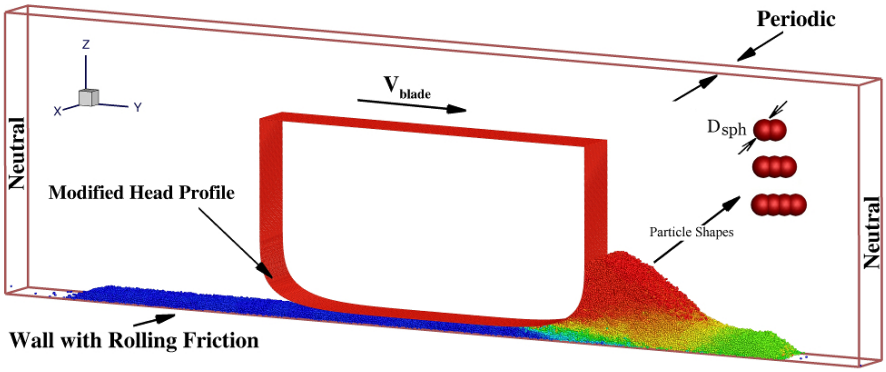

(b)

Figure 1: The device simulation set-up and initial preparations presented for a modified blade profile. (a) The initial bed preparation using a rain fall technique is presented; particles are coloured with their velocity magnitudes and diameters are not to scale for better presentation. (b) The rod-shaped particles with different aspect ratios A_r are presented using a multi-sphere approach. Also, the particles are coloured in a representative simulation with v_y (velocity in y-direction). Only a section of the spreader with a width L_x is simulated by choosing periodic boundary conditions in x-direction and in y-direction neutral walls are used (no interaction with particles).

0.4 and $\rho_{\text{rod}} = 1.3$ gr/cm^3 for all particles which are typical values for PEEK polymeric powders [21]. The spring constant κ_n is calculated from the Young's modulus and Poisson ratio using a characteristic velocity $V_c = V^T_{\text{blade}}$ [22, 1]. The tangential force constants κ_t and γ_t are respectively set to $2/7\kappa_n$ and $1/2\gamma_n$ respectively [22].

2.2 Simulation set-up and post-processing

The rods with various aspect ratios $A_r = 1.5,\ 2.0,\ 2.5$ are created by overlapping spheres with $\ell = 0.5$ (Figure 1b) and number densities of $N_{\text{A}_r} = 0.5,\ 0.3,\ 0.2$ respectively. The initial configuration (before the spreading starts) is prepared by pouring randomly generated particles on the bottom wall (see Figure 1a). This is done within a simulation box with dimensions $L_x = 2.46 \times 10^{-3}$, $L_y = 0.04$ and $L_z = 0.03$. The geometric parameters L_x, L_y and L_z are the width, length and height of the simulation box (red boundaries in Figure 1b). Note that all values are in SI units except otherwise stated. The preparation method is different from the delivery system in LS devices; nevertheless, since the powder is not compacted in the delivery piston and rests under its natural weight, this method of initiating the simulation, is adequate for the current purpose.

The box size in the flow-direction L_y changes to accommodate all the particles as they are spread and the corresponding walls exert no force on the particles (walls labelled neutral in Figure 1b). The number of particles in each simulation is adjusted to supply an initial thickness of $\delta_{init} \approx 10D_{\text{sph}}$ for all particle types, where D_{sph} is the diameter of spheres used to generate the rod-shaped particles. In addition, the blade displacement from the bottom wall, δ_{blade} is set to $5D_{\text{sph}}$ which is the profile's minimum distance to the bottom wall and essentially sets the powder bed thickness.

The solid volume fraction, ϕ_s, is calculated and its maximum value is used as the objective function – which means a more effective spreading process – to optimise the blade profile. The ϕ_s values are calculated using a Voronoi tessellation technique [23] and only a section of the bed away from the edges are considered to suppresses the end effects. This is, in fact, a reasonable assumption since the full extent of the bed in not normally used for fabrication; see [1] for further details.

3 The new blade design

Haeri et al. [1] argued that an "effective" bed-spreader contact, determines the quality of a prepared powder bed (a high ϕ_s and low ϵ), where ϵ is a measure of roughness. Based on visualisations of the bed-spreader contact dynamics they related this to a particle dragging phenomenon which distorts the bed if a spreader type did not provide an effective support for the particle heap that forms in front of the spreader (see Figure 1b). This suggests that a geometric modification of the spreader should in principle, significantly improve the bed's quality.

By modifying the spreader's head profile a new class of spreading devices is suggested.

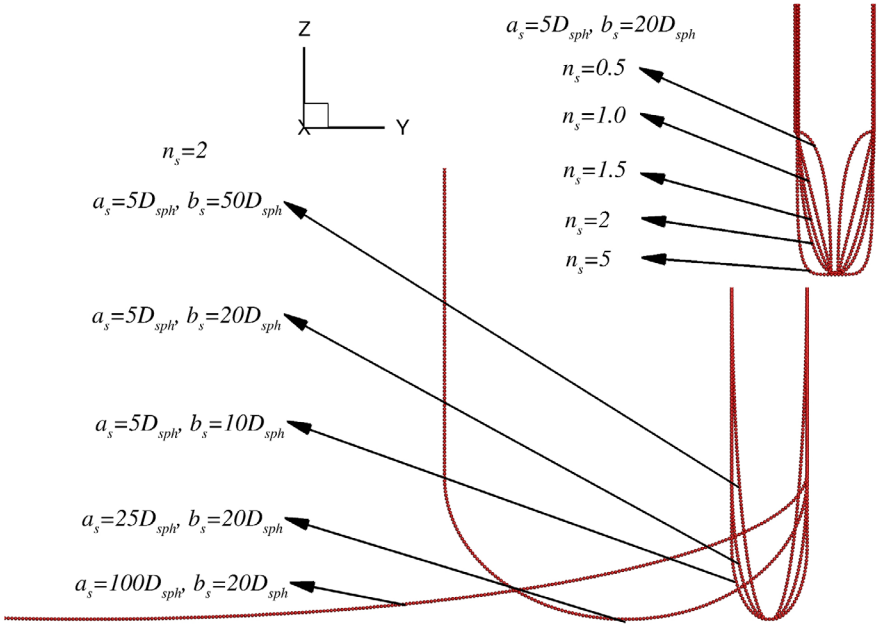

Figure 2: Different spreader profiles used for the optimisation. Only a subset of all designs are presented to show the effects of changing parameters a_s, b_s and n_s. Only half of the widest blade with $a_s = 100D_{\text{sph}}$ is presented.

A super-elliptic profile with three parameters n_s, a_s and b_s is proposed here:

$$\left|\frac{y}{a_s}\right|^{n_s} + \left|\frac{z}{b_s}\right|^{n_s} = 1. \tag{3}$$

The parameters n_s, a_s and b_s respectively, control the overall shape, width and height of the profile. The blade thickness is $w_s = 2a_s$ and its height is $h_s \gg b_s$. Note that the blade's height is longer than b_s and remains a straight line for $z > b_s + \delta_{\text{blade}}$, its value is chosen to be larger than the maximum height of the powder heap formed in front of the blade during the spreading process and has no effect on the optimisation results. In Figure 2 various profile shapes proposed for the optimisation are presented. Three values $(10, 25, 100)D_{\text{sph}}$ and $(10, 20, 50)D_{\text{sph}}$ are chosen for a_s and b_s respectively. The parameter n_s determines the overall shape of the profile. Initially, five different shapes $n_s \in \{0.5, 1.0, 1.5, 2.0, 5.0\}$ are considered (see Figure 2), however, after the initial optimisation a few more values are considered to show that the best identified n_s is in fact the optimum value.

3.1 Optimisation results and discussions

The results of 48 simulations with different optimisation parameters are presented in Figure 3. Before analysing the results any further, it is clear that the blade's geometry

is indeed a major parameter for controlling the bed quality. Figure 3 clearly shows the variation in ϕ_s from low values of $\phi_s \approx 0.4$ to values as high as $\phi_s \approx 0.58$. This proves the effectiveness of geometrical modification of the blade's head profile to maximise ϕ_s and indicates the validity of the initial hypothesis.

For comparison with a straight edge blade, the data from [1] are used. They performed simulations with mono-sized ($\mathrm{A}_r = 1.0 \cdots 2.5$) particles at similar operating conditions. However, they showed that the characteristics of poly-sized beds (with small variation in the aspect ratio) could be approximated by a number density weighted averaging. To find an approximate value for the poly-sized case considered here, a number density average of the mono-sized simulations of [1] is calculated. This can be written by $\phi_s = \sum N_i \phi_s(\mathrm{A}_{r,i})$ which yields a value of $\phi_s = 0.4$ for straight edge blade spreader of a mixture of particles with number densities considered in this paper.

The effects of overall profile shape are demonstrated in Figures 3a to 3e. In these figures, the value of the parameter n_s is changed which characterises the overall shape of the profile. A value of $n_s = 0.5$ generates a concave profile and the results are presented in Figure 3a. Evidently, this profile does not improve the compaction significantly, nevertheless, some improvement is observed especially for the lowest value of blade width of $5D_{\mathrm{sph}}$.

A linear profile can be generated by setting $n_s = 1$. The simulation results for this profile and different width and height parameters a_s and b_s are presented in Figure 3b. The bed quality – as expected – is a function of both profile height and also the spreader width. Generally, shorter (smaller b_s) and wider (larger a_s) profiles generate higher volume fractions ϕ_s. The sensitivity of the linear profile to height is higher for wider designs but almost no dependence on height is observed for narrow designs ($a_s = 5D_{\mathrm{sph}}$). It is also interesting to note that ϕ_s dependence on a_s for the concave profile ($n_s = 0.5$) is opposite to that of the linear profile and all the other convex profiles. It is believed that for a concave profile ($n_s = 0.5$) some particles may get clogged in the hollow region between the blade's head profile and the bottom surface (or the previous layers). Therefore, wider profiles generate smaller volume fraction for the $n_s = 0.5$ case whereas increasing a_s improves the quality for all other convex profiles (with $n_s \geq 1$).

Figures 3c to 3e show as the value of n_s increases from $n_s = 1.5$ to $n_s = 5.0$, for all the corresponding values of b_s and a_s the volume fraction increases indicating a better quality. In addition, the sensitivity to b_s also decreases such that for $n_s = 5.0$ the volume fraction is practically independent of b_s. This perhaps is not surprising since larger n_s values cause a condensation of curvature very close to the edges and the remaining sections of profile away from the edges are essentially straight lines. Therefore, changing b_s does not significantly change the profile characteristics. For all values of $n_s \geq 1$ wider profiles generate beds with larger ϕ_s. The current results show that optimisation of the profile is highly successful and ϕ_s for $n_s = 5.0$, $a_s = 100D_{\mathrm{sph}}$ and $b_s = 10D_{\mathrm{sph}}$ approaches a value of $\phi_s = 0.58$. This value is close to the critical volume fraction of spherical frictional particles (with $\mu_c = 0.5$) determined as $\phi_c = 0.587$ by Chialvo et al. [24]. Therefore, any

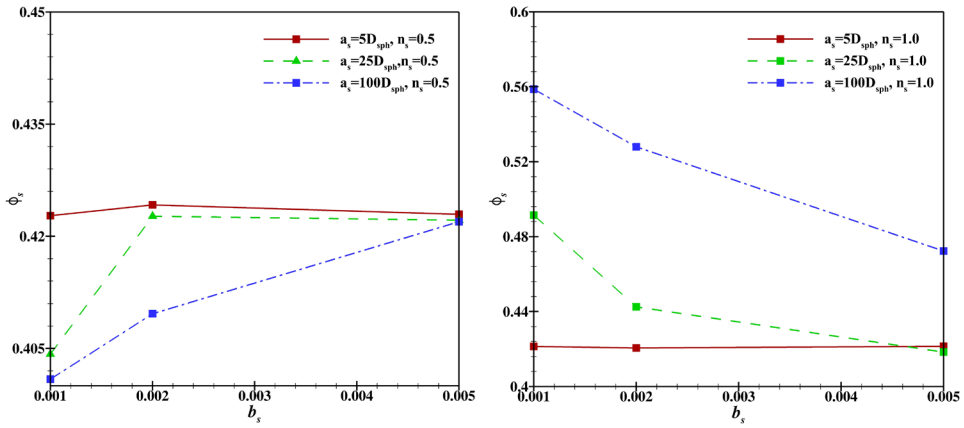

(a) $n_s = 0.5$

(b) $n_s = 1.0$

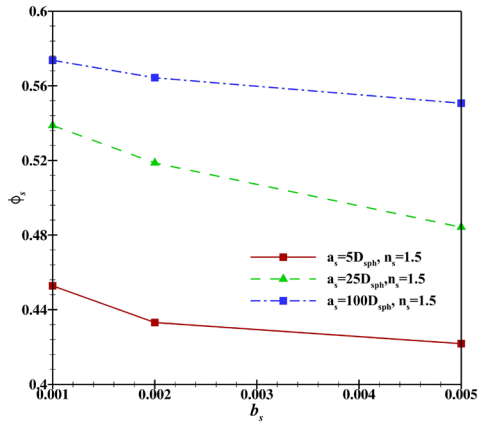

(c) $n_s = 1.5$

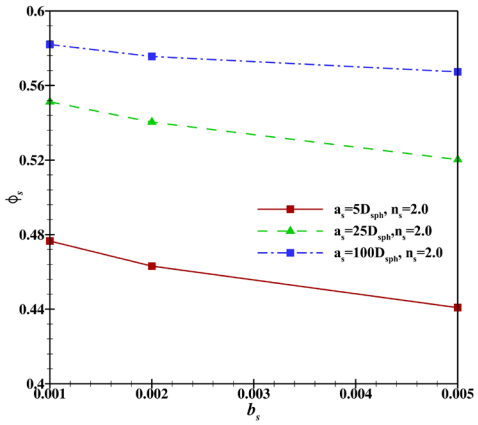

(d) $n_s = 2.0$

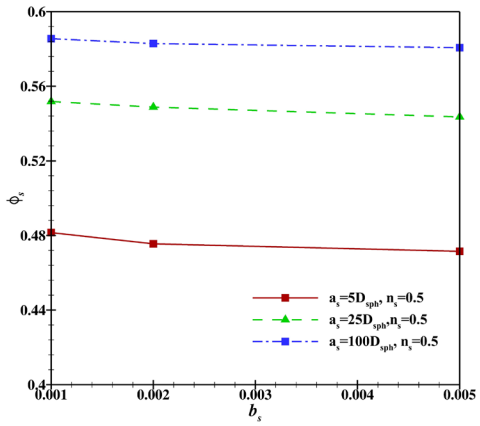

(e) $n_s = 5.0$

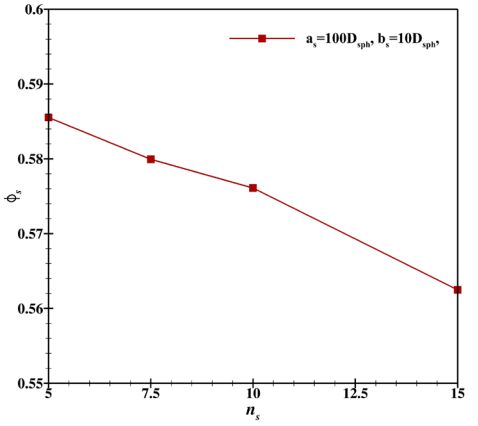

(f) Optimum n_s

Figure 3: Variations in solid volume fraction ϕ_s with different optimisation parameters. The values on b_s axis correspond to $(10, 20, 50) \times D_{\text{sph}}$.

further compaction without significant compression of the bed is not expected.

For the particular powder considered here (with the specified material and morphology characteristics) a larger ϕ_s is obviously not anticipated and hence further optimisation is redundant. Nevertheless, since the ϕ_s monotonically increased during the optimisation process (see Figure 3a to Figure 3e), a valid question is whether ϕ_s versus n_s curve has a plateau and one can choose an arbitrarily large n_s, or an optimum n_s value actually exists. It is important to note that as $n \to \infty$ the profile will approach a typical rectangular shape which as demonstrated in [1] significantly degrades the bed quality. Therefore, the existence of an optimum value for n_s is certain. To show that $n_s = 5.0$ is in fact that optimum value and generates the highest ϕ_s a series of the simulations with 3 other values of $n_s \in \{7.5, 10.0, 15.0\}$ are performed. The results are presented in Figure 3f which proves that $n_s = 5.0$ (noting the resolution of the current parametric study) must be the optimum profile shape.

In this section, the profile with parameters $n_s = 5.0$, $a_s = 100D_{\text{sph}}$ and $b_s = 10D_{\text{sph}}$ is identified as the optimum profile. A value of $b_s = 10D_{\text{sph}}$ $(= 1mm)$ may not be feasible to manufacture. However, noting the independence of ϕ_s from b_s in Figure 3e, one can choose a larger value of b_s to manufacture a spreader with more realistic physical dimensions.

4 Conclusion

In this paper it is first demonstrated that geometric optimisation of a blade type spreader can significantly improve the quality of a powder bed (a higher ϕ_s) that is generated by spreading for Particle Bed Fusion (PBF) processes. A new class of spreading devices is proposed by assuming a super-elliptic edge profile with three different parameters controlling width, height and the overall shape of the profile. A set of 48 device-scale DEM simulations are performed and the optimum values for these parameters are identified. It is shown that this optimisation is highly effective and packings close to the critical volume fraction is achievable. Therefore, the optimised blade is as effective as a roller. This could greatly reduce the production and maintenance costs of the PBF devices by obviating the need for significantly more expensive and complex spreading devices.

Acknowledgement

This work was supported by the Institution of Mechanical Engineers (IMechE) award EAC/KDF/OFFER/17/065. The author also gratefully acknowledges the use of ARCHER – The UK National Supercomputing Service (http://www.archer.ac.uk) – for conducting the simulations under the EPSRC's Resource Allocation Panel (RAP) Grant E504.

References

[1] S. Haeri, Y. Wang, O. Ghita, and J. Sun. Discrete element simulation and experimental study of powder spreading process in additive manufacturing. *Powder Technology*, 306:45–54, 2017. ISSN 0032-5910. doi: 10.1016/j.powtec.2016.11.002.

[2] I. Gibson and D. Shi. Material properties and fabrication parameters in selective laser sintering process. *RTejournal 3: Forum Rapid Technol.*, 1995.

[3] Y. Shi, Z. Li, H. Sun, S. Huang, and F. Zeng. Effect of the properties of the polymer materials on the quality of selective laser sintering parts. *IMechE Journal*, 218:247–253, 2004.

[4] R. D. Goodridge, K. W. Dalgarno, and D. J. Wood. Indirect selective laser sintering of an apatite-mullite glass-ceramic for potential use in bone replacement applications. *Proceedings of the Institution of Mechanical Engineers, Part H*, 220:57–68, 2006.

[5] L. Hao, M. M. Savalani, Y. Zhang, K. E. Tanner, and R. A. Harris. Effects of material morphology and processing conditions on the characteristics of hydroxyapatite and high-density polyethylene biocomposites by selective laser sintering. *Journal of Materials: Design and Applications*, 220:125–137, 2006.

[6] S. Ziegelmeier, P. Christou, F. Wöllecke, C. Tuck, R. Goodridge, R. Hague, E. Krampe, and E. Wintermantel. An experimental study into the effects of bulk and flow behaviour of laser sintering polymer powders on resulting part properties. *Journal of Materials Processing Technology*, 215:239–250, 2015.

[7] P. A. Cundall and O. D. L. Strack. A discrete numerical model for granular assemblies. *Geotechnique*, 29:47–65, 1979.

[8] E. Onate and D. R. J. Owen. *Particle-Based Methods: Fundamentals and Applications, Computational Methods in Applied*. Springer, 2011.

[9] T. I. Zohdi. Computation of the coupled thermo-optical scattering properties of random particulate systems. *Computer Methods in Applied Mechanics and Engineering*, 195:5813–5830, 2006.

[10] T. I. Zohdi. Rapid simulation of laser processing of discrete particulate materials. *Archives of Computational Methods in Engineering*, 20:309–325, 2013.

[11] T. I. Zohdi. Additive particle deposition and selective laser processing – a computational manufacturing framework. *Computational Mechanics*, 54:171–191, 2014.

[12] Z. Xiang, M. Yin, Z. Deng, X. Mei, and G. Yin. Simulation of forming process of powder bed for additive manufacturing. *Journal of Manufacturing Science and Engineering*, 138:081002, 2016.

[13] J. C. Steuben, A. P. Iliopoulos, and J. G. Michopoulos. Discrete element modeling of particle-based additive manufacturing processes. *Computer Methods in Applied Mechanics and Engineering*, 305:537–561, 2016.

[14] S. A. Khairallah, A. T. Anderson, A. Rubenchik, and W. E. King. Laser powder-bed fusion additive manufacturing: Physics of complex melt flow and formation mechanisms of pores, spatter and denudation zones. *Acta Materialia*, 108:36–45, 2016.

[15] A. Rai, H. Helmer, and C. Korner. Simulation of grain structure evolution during powder bed based additive manufacturing. *Additive Manufacturing*, 13:124–134, 2017.

[16] S. Plimpton. Fast parallel algorithms for short-range molecular dynamics. *Journal of Computational Physics*, 117:1–19, 1995.

[17] Y.C. Zhou, B.D. Wright, R.Y. Yang, B.H. Xu, and A.B. Yu. Rolling friction in the dynamic simulation of sandpile formation. *Physica A*, 269:536–553, 1999.

[18] J. Ai, J.-F. Chen, J.M. Rotter, and J.Y. Ooi. Assessment of rolling resistance models in discrete element simulations. *Powder Technology*, 206:269–282, 2011.

[19] C.M. Wensrich and A. Katterfeld. Rolling friction as a technique for modelling particle shape in dem. *Powder Technology*, 217:409–417, 2012.

[20] A. Di Renzo and F.P. Di Maio. Comparison of contact-force models for the simulation of collisions in dem-based granular flow codes. *Chemical Engineering Science*, 59: 525–541, 2004.

[21] ully. A comprehensive review of the materials properties of victrex® peek™ high performance polymer. enzo, VICTREX, 2016.

[22] J. Shäfer, S. Dippel, and D. Wolf. Force schemes in simulations of granular materials. *Journal de Physique I*, 6:5–20, 1996.

[23] C. H. Rycroft. Voro++: A three-dimensional voronoi cell library in c++. *Chaos: An Interdisciplinary Journal of Nonlinear Science*, 19:041111, 2009.

[24] S. Chialvo, J. Sun, and S. Sundaresan. Bridging the rheology of granular flows in three regimes. *Physical Review E*, 85:023305, 2012.